18

Electron spin resonance of $NV^{(-)}$-centers in synthetic fluorescent diamond microcrystals under conditions of optical spin polarization

© V.Yu. Osipov[1], K.V. Bogdanov[2], A. Rampersaud[3], K. Takai[4], Y. Ishiguro[5], A.V. Baranov[2]

[1] Ioffe Institute,
194021 St. Petersburg, Russia
[2] ITMO University,
197101 St. Petersburg, Russia
[3] Columbus Nanoworks Ltd., Columbus,
43212 Ohio, United States
[4] Department of Chemical Science and Technology, Hosei University, Koganei,
184-8584 Tokyo, Japan
[5] Department of Electrical and Electronic Engineering, Tokyo Denki University,
120-8551 Tokyo, Japan

e-mail: osipov@mail.ioffe.ru

Received October 25, 2022
Revised November 15, 2022
Accepted November 15, 2022.

Electron paramagnetic resonance (EPR) spectra of synthetic diamond microcrystals with $NV^{(-)}$-centers have been studied. It is shown that under the conditions of irradiation of the material with the light of a xenon lamp at low temperatures ~ 100 K, the intensities of the EPR signals corresponding to the „forbidden“ ($\Delta m_s = 2$) and low field allowed ($\Delta m_s = 1$) transitions are amplified several times, while the EPR signals from paramagnetic nitrogen and impurity nickel in the charge state -1 practically do not change. This is due to a change in the population of levels of the ground triplet state of the $NV^{(-)}$- center and the optical polarization of spins in the state $m_s = 0$ of the triplet level.

Keywords: nitrogen-vacancy centers, synthetic diamond, electron paramagnetic resonance, spin polarization, luminescence.

DOI: 10.21883/EOS.2022.12.55255.4248-22

Introduction

Diamond is wide-gap material with a gap of 5.45 eV, which can currently be easily synthesized by various methods, including the static method under high pressures (5−7 GPa) and temperatures (> 1350°C) and the chemical vapor deposition method from carbon or carbon-containing precursors. Defects in diamonds have been studied since the mid-1950s. To date, up to 200−250 point defects and various complexes composed of elementary subunits are known in diamonds. Their description is givenin the reference book on the optical properties of diamond [1]. All defects/centers can be conditionally divided into two groups: optical and paramagnetic. Optical centers usually include centers that are characterized by specific luminescence in the ultraviolet and visible ranges of the spectrum (or by specific absorption), while paramagnetic centers that are demonstrating specific signals of electron paramagnetic resonance (EPR). And only a small part of the centers simultaneously have both sets of identification optical and paramagnetic signatures. Among such a centers is nitrogen-vacancy pair $NV^{(-)}$ in a negatively charged state [2,3].

It should be noted that the main studies on paramagnetic and optical centers in diamonds, including those induced by radiation damage from high-energy radiation, were carried out before the mid-1970-s, as described in the review by Loubser and van Vyk [4]. The vast majority of „new“ centers in diamonds were discovered, identified or redefined during the 1990-s by international consortiums of researchers from different countries [5–7]. At the same time, nickel and its numerous combinations with nitrogen, vacancies and elemental hydrogen, as well as other heteroelements, including elements of the carbon subgroup, led to the appearance of a whole assembly of optical and paramagnetic centers from the very beginning of the 2000-s and up to the present time [7–12]. At the same time, it should be noted that most of the known centers in diamond are magnetically inactive and cannot be detected by EPR-spectroscopy. Among these magnetically inactive („hidden“) centers there are neutral nitrogen pairs NN (A-centers), NVN (H3-centers), 4NV (B-centers), etc. [13]. Paramagnetically inactive are often complex centers obtained by arrangement elementary defects in crystals during treatment at high temperatures above 1400°C. The process associated with such a rearrangement and coalescence of defects also causes discoloration of diamond crystals, which

is used in the manufacture of synthetic gem-quality diamond crystals. Explosion of concern in the study of NV-centers arose in the mid-2000s and was initially associated with the great potential associated with the development of single-photon light sources and modulation of the emission radiation of these centers for telecommunications and information processing tasks [14,15]. The attractiveness of these centers for practice was also due to the fact that the electronic terms of these centers were well defined and confirmed by the results of theoretical analysis within the six-electron model [3]. However, this is not completed the main scientific attraction of systems based on optical $NV^{(-)}$-centers.

Diamond crystals with nitrogen-vacancy centers in charge states 0 and -1, which give intense fluorescence in the green and red regions of the spectrum, are promising sensors for a number of physical fields and influences, such as magnetic field, microwave radiation of a certain frequency, temperature and mechanical strains due to the peculiarities of the electronic structure of the energy levels of $NV^{(o)}$ and $NV^{(-)}$- centers providing optical emission [16–22]. Thus, in particular, the parameters of the electronic levels of the ground ($^3A_2$) state of the $NV^{(-)}$-center substantially depend on the intracrystalline mechanical strains [22]. Diamond nanoparticles with $NV^{(-)}$ are successfully used for contouring and visualization of intracellular organelles and tracking the movement of single organelles and neurons with a spatial resolution of at least 15 nanometers [23]. Synthetic diamond microcrystals with $NV^{(-)}$-centers smaller than $20-30\,\mu$m are the most interesting for use as sensors when combined with fiber optics elements, because can be easily placed as sensitive or active elements at the ends of single- and multimode optical fibers and/or in the core of these fibers [24].

$NV^{(-)}$-centers with charge status -1 are well identified in diamond microcrystals by electron paramagnetic resonance and luminescence. In the EPR spectra, they show narrow lines corresponding to the so-called allowed and „forbidden“ transitions, and the intensities and widths of the lines of allowed transitions turn out to be the most sensitive to the size of diamond crystallites and the quality of the diamond lattice in the size range $5-100$ nm [25]. For diamond particles smaller than 20 nm, the lines of allowed transitions almost completely disappear, while the EPR lines from „forbidden“ transitions remain [26].

Some features of the EPR spectra of $NV^{(-)}$-centers have already been discussed in the literature for synthetic micro- and nano-crisralls of type Ib [25,26]. In particular, we studied the intensity saturation of the EPR lines of allowed and „forbidden“ transitions in $NV^{(-)}$-centers as a function of the microwave power [27].

An urgent task at present is the development and improvement of complex methods for diagnosing diamond micro- and nanocrystals with $NV^{(-)}$- centers and evaluation of their crystalline quality, which allow selecting a synthesized material with premium characteristics to create sensors, light emitters and active elements [28,29]. Among such diagnostic methods is the study of the EPR spectra of diamond microcrystals under conditions of optical spin polarization.

Samples and methods

In present work, microcrystals of synthetic Ib HPHT diamond manufactured by Columbus Nanoworks Ltd. (USA) were studied. Microcrystals were grown under conditions of high pressures (> 5 GPa) and high temperatures ($> 1300^\circ$C) using a nickel-containing metal-catalyst The size of initial crystals with a good faceting varied in the range of $200-350\,\mu$m. $NV^{(-)}$-centers were created by irradiating synthesized microcrystals with a beam of high-energy (> 2 MeV) electrons (absorbed dose $\sim 6\times10^{18}\,e^-/cm^2$) followed by annealing in an inert atmosphere at a temperature 800°C within 6 hours. Microcrystals were further processed in boiling acids. The fabricated material has been given the unique name #7381. The resulting fluorescent microcrystals with $NV^{(-)}$- centers were then powdered in a planetary mill in inert atmosphere (using steel balls) to an average size of $\sim 13\,\mu$m and were cleaned in boiling acids from metal inclusions and related contaminants. The particle size in the ensemble varied from ~ 4 to $35\,\mu$m. Further, in order to remove surface defective regions in the sp^2-hybridized state, i.e. non-diamond forms of carbon, the resulting powders were subjected to gas-phase etching by oxidation in air for 1 hour at temperature of 450°C. Details of the procedures for irradiation and grinding of diamond microcrystals for a number of cases can also be found in the works [30–32]. The concentration of $NV^{(-)}$-centers in the fabricated microcrystals was ~ 3.8 ppm, and the substitutional nitrogen, i.e. the main dopant of synthetic diamond was 140 ± 10 ppm. The impurity nickel content in the material was no more than 5 ppm. At temperatures below 140 K, the nickel atoms present in the crystal in the carbon-substituting positions were in a negative charged state. The processed and purified milled microcrystals were a white powder. Photos of initially microcrystals with $NV^{(-)}$- centers, shoted in the mode of registration of fluorescence excited by radiation with a wavelength of 532 nm, are shown in Fig. 1, *a*, and the powder of milled microcrystals is shown in Fig.1, *b* (tube *1*). The manufactured sample, obtained by milling, was given the unique designation #7381-*b*.

The EPR spectra in the temperature range $90-100$ K at a microwave frequency ~ 9.04 GHz were studied by JEOL-JES-FA300 EPR spectrometer (Japan) which was equipped with flow-type cryostat by Oxford Instruments (Great Britain) and an optical window for illumination with UV visible light. For cooling to a temperature of 90 K, liquid nitrogen vapor was used as a coolant. Temperature stabilization in the temperature range $90-100$ K was carried out with an accuracy of 0.03 K. The sample

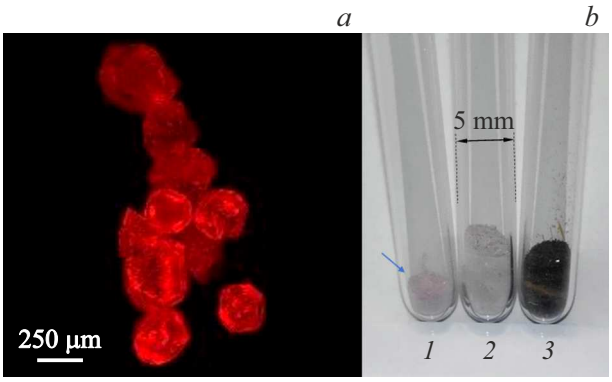

Figure 1. Fluorescent image of ten synthetic diamond microcrystals #7381 with $NV^{(-)}$-centers, obtained using an epifluorescence microscope a filter with bandwidth of 590–650 nm and an illuminating laser with wavelength of 532 nm, as well as an optical image of the powder of milled #7381-*b* microcrystals in a quartz tube (left) in comparison with other diamond micro- and nanomaterials (*b*). Panel (*a*): intense red glow indicates the presence of $NV^{(-)}$-centers; particle size is 250–300 μm. Panel (*b*), ampoules with materials: *1* is diamond powder #7381-*b*, *2* is reference powder of 10-μm of fluorescent diamond with $NV^{(-)}$, *3* is 5-nm detonation diamond powder with $NV^{(-)}$-centers at a concentration less than 1 ppm.

was illuminated with a 500 W xenon discharge lamp (Ushio Lighting Inc.) through an HA30 glass optical filter (bandwidth 300–900 nm) by Hoya Candeo Optronics Corporation (Saitama, Japan). Illumination through this filter did not cause any significant heating of the sample at cryostat temperature of 100 K. To change the spectral composition of the radiation, Hoya L42 and R64 cutoff optical filters with cutoff wavelengths of about 420 nm and 640 nm were additionally used. The EPR spectra were recorded under conditions without illumination and with illumination. The illumination parameters did not change during the recording of the EPR spectra. The following parameters were used to record the spectra: magnetic field modulation 0.07 mT, modulation frequency — 100 kHz, gain — 500, time constant — 30 ms, number of accumulations of spectra for averaging and noise reduction in signals — 8. The microwave power was chosen equal to 0.003 mW or from the range of 0.001–0.01 mW.

Luminescence spectra were recorded using the „inVia“ micro-Raman setup (by Renishaw, UK) using exciting laser radiation at wavelength of 488 nm and 50^x micro objective focusing radiation into 2 μm diameter spot on the surface of a single microcrystal or its fragment. Luminescent radiation was collected in backscattering geometry from the sample surface. Due to the high fluorescence intensity of the particles under study, the intensity of the exciting radiation was chosen to be 0.0001% of the maximum achievable on the sample surface in the setup used ($\sim$ 5–8 mW). The characteristic spectrum was obtained by statistical averaging of data collected from ten micro crystals. The Raman spectra of microcrystals were recorded at 0.5% (of the maximum achievable) intensity of the exciting radiation.

Experimental results and discussion

The fluorescence spectrum of sample #7381 at room temperature is shown in Fig. 2. It has all the characteristic features associated with the emission of $NV^{(-)}$- centers, namely: zero-phonon line at 638 nm and a broad long-wavelength band associated with phonon repetitions extending up to $\sim$ 800 nm and even further. The narrow Raman line centered at 1332 cm^{-1} and 3.4 cm^{-1} wide (the width of the instrumental function of the spectrometer is 1.6 cm^{-1}) indicates a sufficiently high quality of the diamond lattice and the absence of mechanical strains in the lattice from interstitial impurities (see inset in Fig. 2). Fluorescent bands and lines associated with NV- centers in the neutral state are absent in the spectrum in Fig. 2, which indicates the predominant (up to 98%) occurrence of NV- centers in sample #7381 in a negatively charged state.

The energy diagram of the electronic terms of the main optical centers ($NV^{(-)}$ and $NV^{(o)}$) and donor impurities (isolated nitrogen atoms) of irradiated and annealed diamond is shown in Fig. 3, *a*, and Fig. 3, *b* shows the splitting scheme of the sublevels of the $^3A_2$ triplet state in a magnetic field in situations when the magnetic field is directed parallel to the axis of the NV center. Additional details of the energy diagram can be found in work of Sabedi et al. [33]. The $^3A_2$ state is the ground unexcited state of the $NV^{(-)}$-center and, therefore, the final state for all radiative and nonradiative recombination channels, caused by optical excitation of this

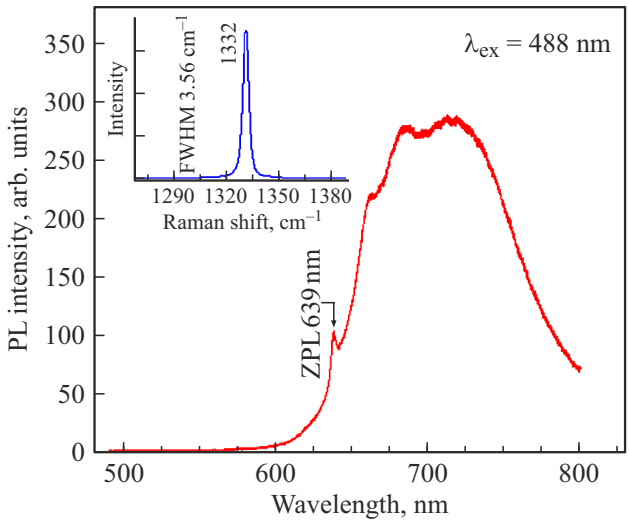

Figure 2. Luminescence spectrum of synthetic diamond microcrystals #7381 with $NV^{(-)}$-centers. The excitation was performed by laser radiation 488 nm. The intensity of the exciting radiation on the sample was 0.0001% of the maximum, corresponding to a power of 5–8 mW. Temperature T = 293 K. Inset: Raman spectrum taken at 0.5% excitation intensity.

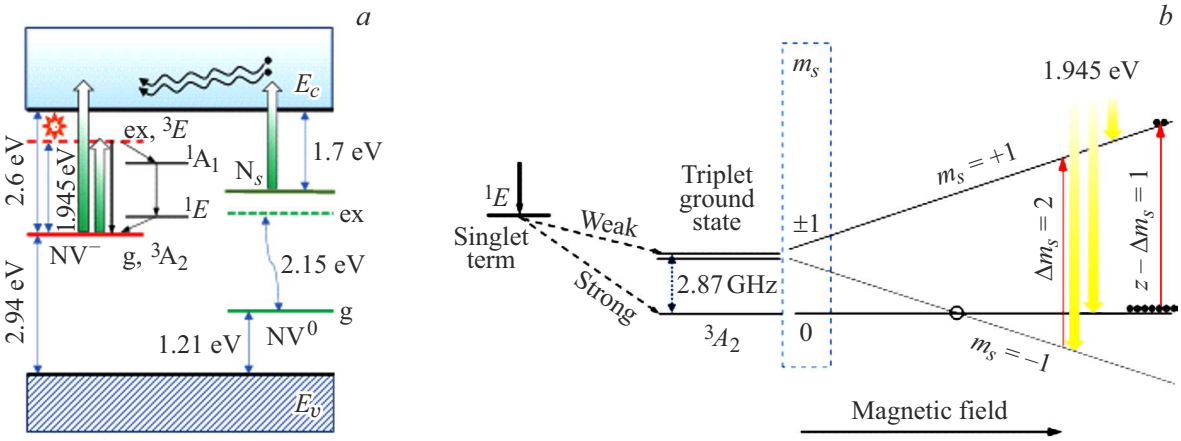

Figure 3. Scheme of energy levels of $NV^{(-)}/NV^{(o)}$ centers and substitutional nitrogen impurities in the band gap of diamond (*a*) and Zeeman splitting of the levels of the ground state $^3A_2$ of the $NV^{(-)}$-center in a magnetic field (*b*). Designations: *g*-, *ex*-main ($^3A_2$) and excited (^3E) triplet states, E_v, E_c are the edges of the valence and conduction bands, $^1A_1$ and ^1E-singlet electronic levels of the $NV^{(-)}$-center, separated from the level $^3A_2$ by 0.44 and 1.63 eV [1]. m_s is magnetic quantum number of the ground state sublevel in the triplet center. The energy gap between sublevels $m_s = 0$ and $m_s = \pm 1$ in zero field is given in units of GHz. The wide and narrow vertical arrows show the optical transitions associated with the absorption and emission of radiation.

center, but the sublevels of the $^3A_2$ triplet differently affect the radiative recombination channels and luminescence in the case of applying a magnetic field greater than 50 mT. The luminescence intensity is maximum in the case of a zero external magnetic field and decreases significantly (by 15–17%) in the case of self-crossing of $^3A_2$ sublevels in a field of $\sim$ 100 mT [24].

EPR spectra under dark conditions

The powder EPR spectrum of irradiated and annealed #7381-*b* diamond microcrystals consists of a set of signals (signatures) corresponding to impurity defects and triplet optical centers. The EPR spectrum of the #7381-*b* sample, recorded fragmentarily at $T = 100$ K under dark conditions, is shown in Fig. 4, *a, b* (curve *1*) for different magnetic field ranges. It consists of narrow lines of allowed ($\Delta m_s = 1$) and „forbidden“ ($\Delta m_s = 2$) transitions in $NV^{(-)}$-centers, a triplet signal from substitutional nitrogen impurities with electron spin 1/2 and nuclear magnetic moment $I = 1$, and a singlet signal from substitutional nickel impurities with spin 3/2 in the charge state −1 [5,34,35]. The triplet signal from nitrogen (with a hyperfine structure due to the magnetic moment of the nucleus ^{14}N) is located in the range of magnetic fields 313–334 mT (*g*-factor of the central component $g = 2.0024$, line width $\Delta H_{pp} = 0.099$ mT). The singlet signal from a negatively charged nickel impurity in the substitutional position ($S = 3/2$, $g = 2.0319$) is located near the low-field component of the nitrogen triplet and is well resolved [5]. The parameters of the triplet ($g = 2.0024$) and singlet ($g = 2.0319$) signals, analyzed by the previously described method of double integration of the EPR spectrum [36], correspond to neutral nitrogen and nickel concentrations of about 140 ppm and 4.3 ppm. Allowed transitions from $NV^{(-)}$- centers are represented in the powder spectrum by two pairs of symmetrically arranged lines with indices *z* and *x*, *y* for different orientations of the NV-center axis relative to the direction of the magnetic field for the magnetic field ranges $H < 313$ mT and $H > 334$ mT. The high-field signal components of $NV^{(-)}$-centers located in the range $H > 334$ mT are not specifically shown in Fig. 4, *a*. Scheme of the Zeeman splitting of the energy levels of the $^3A_2$ triplet state together with allowed and „forbidden“ microwave transitions $\Delta m_s = 1$ and $\Delta m_s = 2$ is shown in Fig. 5 for various orientations of the axis [1] of $NV^{(-)}$-center relative to the direction of the magnetic field. For such a scheme, centers with axes making angles 0°, 54.7° and 109.5° with the magnetic field vector [37] are chosen. From this scheme, the picture of the arrangement of lines in the EPR powder spectrum of an ensemble of randomly oriented in space $NV^{(-)}$- centers is clear. In the range of magnetic fields 210–290 mT, the main contribution to the powder spectra comes from $NV^{(-)}$-centers oriented predominantly orthogonally to the direction of the magnetic field (with an accuracy of ±20°). The registered powder spectrum is obtained by angular averaging of the individual EPR spectra of $NV^{(-)}$- centers with different orientations of the crystallographic axes as a whole over the ensemble.

Signals from triplet $NV^{(-)}$- centers have a very low intensity compared to the signal for paramagnetic nitrogen and correspond to an $NV^{(-)}$ concentration of $\sim$ 3.8 ppm. Note that, according to the literature data, concentrations of $NV^{(-)}$-centers in diamond crystals above 15–17 ppm are practically not realized. This is due to the difficulty of creating a large number of vacancies (more than 80–100 ppm) in diamond microcrystals without worsening their general crystalline properties due to irradiation with

[1] The axis of the NV-center is collinear to the direction [111] in a cubic diamond crystal. In a crystal, therefore, there are centers with 4 different orientations: [111], [1 1 -1], [1 -1 1], [-1 1 1].

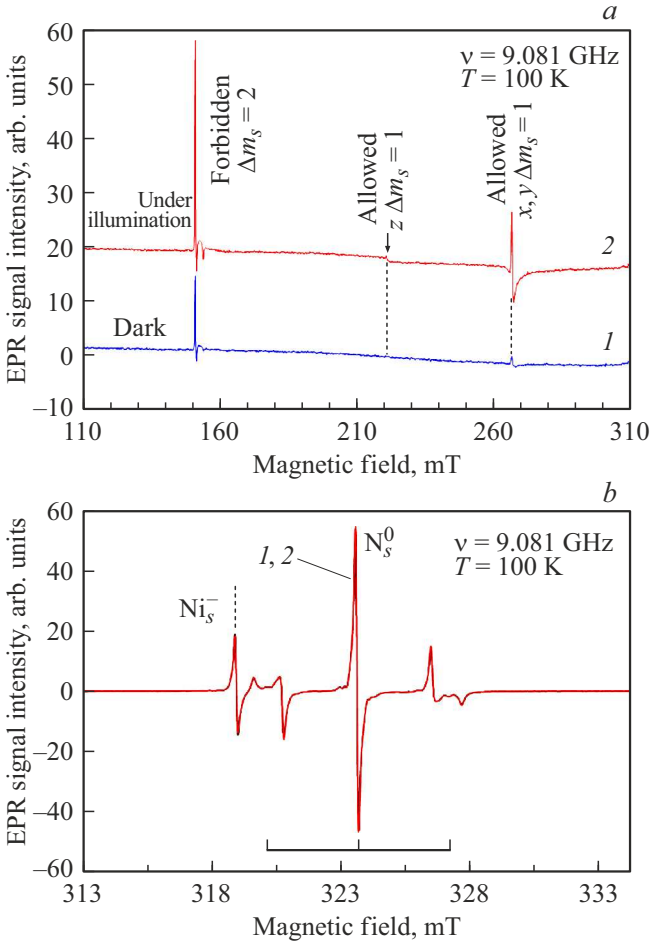

Figure 4. EPR spectra of microcrystals of synthetic HPHT Ib diamond (#7381-*b*) with NV$^{(-)}$-centers under dark conditions (curve *1*) and under illumination (curve *2*) in the ranges of magnetic fields 110−310 mT (*a*) and 313−334 mT (*b*). Temperature $T = 100$ K. Microwave frequency ≈ 9.081 GHz. $P_{MW} = 0.003$ mW. Irradiation was carried out with xenon lamp light passed through Hoya HA30 and L42 filters. For purposes of comparison, the spectra on the panel (*a*) are spaced vertically.

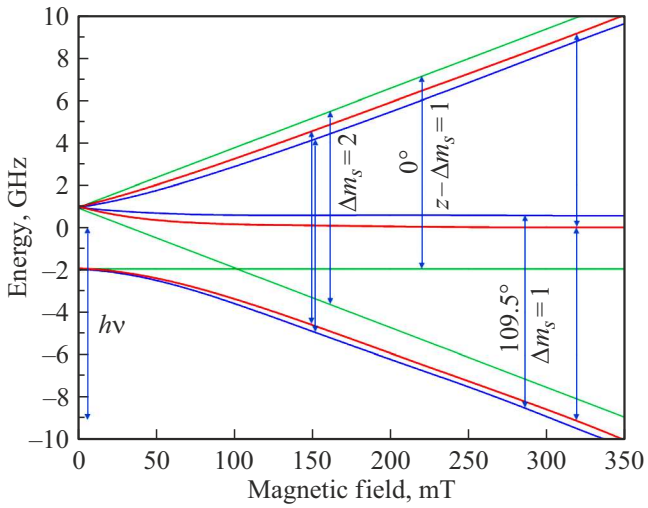

Figure 5. Scheme of the Zeeman splitting of levels of the ground triplet state $^3A_2$ with possible allowed and „forbidden“ microwave transitions $\Delta m_s = 1$ and $\Delta m_s = 2$ for different orientations of the NV$^{(-)}$-center axis relative to the direction of the magnetic field (0°, 54.7° and 109.5°). The transitions are indicated for the microwave frequency 9.05 GHz. The green, red and blue lines correspond to the angles between the NV axis and the field direction equal to 0°, 54.7° and 109.5° respectively.

fast electrons. Although a significant degradation of crystals associated with the aggregation of vacancies into clusters begins at high doses of irradiation, the crystalline quality of the covalent lattice begins to decrease with increasing exposure time of microcrystals to high-energy electrons, starting from doses of the order of 3×10^{19} e/cm^2, while the imperfection associated with defect complexes increases, which affects the decrease in the luminescence yield [29]. Defectivity at the microscopic level is easily controlled by the EPR method by measuring the saturation of „narrow“ signals from paramagnetic impurities or NV$^{(-)}$-centers.

The dependences of the signal amplitudes of allowed transitions (for x, y-components) in NV$^{(-)}$ on the microwave power were studied in the work [27]. It was found that the crystal quality of $\sim$ 15-μm diamond particles is higher than for 100-nm particles specially obtained from the former by mechanical grinding.

EPR spectra under illumination

When the sample is illuminated with broadband light from a xenon lamp, the EPR spectrum changes: it practically does not change (with an accuracy of 2%) in the central range 313−334 mT, i.e. in the region where the triplet signal from paramagnetic nitrogen with spin 1/2 (the so-called P1-centers) and the singlet signal from nickel impurities Ni_s^- are located (Fig. 4, *b*, curve *2*), and is significantly enhanced for lines of „forbidden“ and allowed transitions NV$^{(-)}$- centers in the low-field range 110−310 mT (Fig. 4, *a*, curve *2*). Under the mode of illumination of the sample, the peak intensities of the transition lines $\Delta m_s = 2$ are amplified by a factor of 2.5−3, and the line intensities x, y-$\Delta m_s = 1$ transitions are amplified by more than 5−6 times that is by a greater number of times (Fig. 6, *a,b*). It is noteworthy that the intensities of transitions associated with different energy levels in the energy structure of the triplet of the ground state $^3A_2$ are amplified by a different number of times, which does not allow us to consider the possible cause of the observed effect, an increase in the number of NV$^{(-)}$-centers due to the ionization of a small part of the neutral nitrogen centers present in the crystal, with the transition of electrons to the conduction band of diamond and their subsequent capture by neutral NV$^{(o)}$-centers with changing charge status. In addition, the emergence of „new“ NV$^{(-)}$ from NV$^{(o)}$ as a result of electron charge capture from donors is impossible due to the almost complete absence of neutral NV$^{(o)}$- centers in crystallites according to the data of photoluminescence measurements at room temperature, as well as the invariance of the concentration of Ni_s^-- centers

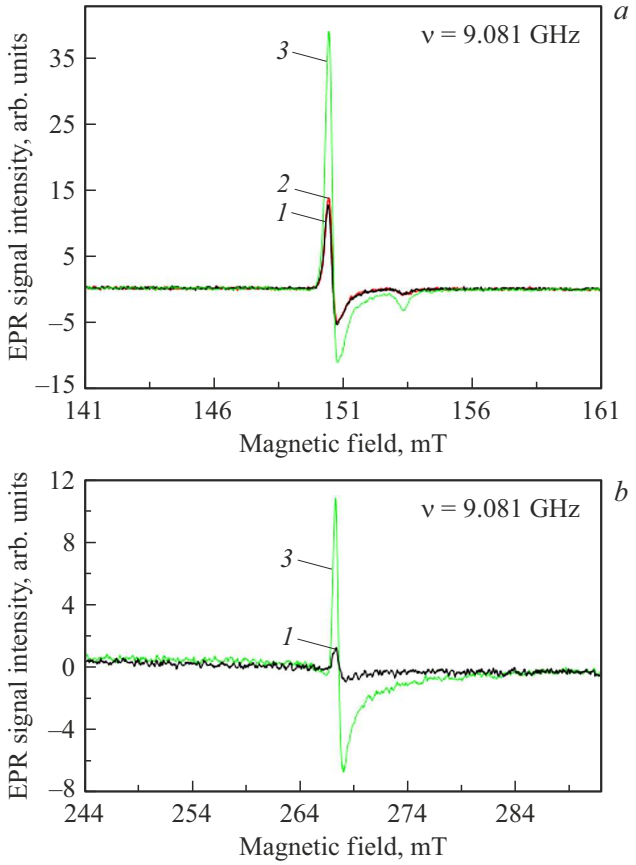

Figure 6. EPR spectra of #7381-*b* microcrystals in the magnetic field ranges 141−161 mT (*a*) and 244−292 mT (*b*), demonstrating „forbidden" ($\Delta m_s = 2$) and low-field allowed (x, y $\Delta m_s = 1$) microwave transitions under dark conditions (curve *1*) and when illuminated by xenon lamp light passed through filters (curves *2* and *3*). Curves *2* and *3* correspond to the radiation that passed through the Hoya HA30, R64 and HA30, L42 filters. Temperature $T = 100$ K. Microwave frequency ≈ 9.08 GHz. $P_{MW} = 0.003$ mW.

and N_s- centers (with an accuracy of 2%) when illuminated by xenon lamp light. Electronic charge transfer from $\sim 2\%$ isolated nitrogen impurities in the amount of ~ 140 ppm to charge storage state could give a hypothetical increase $S = 1\,NV^{(-)}$-centers in the material by ~ 3 ppm if $NV^{(o)}$ were in the material in excess of this value. However, these scenarios are not implemented in practice.

The selective amplification of EPR lines from $NV^{(-)}$-centers is apparently associated with - features of their electronic structure and a change in the population of sublevels of the triplet ground state $^3A_2$ centers illuminated by short-wavelength light from a xenon lamp. Change in populations of sublevels of the triplet state of the $NV^{(-)}$-center under illumination in a magnetic field, leading to an increase in the EPR signal from the low-field component z- $\Delta m_s = 1$, is well known [38]. It is explained by the predominant population of the $m_s = 0$ state during lighting (compared to the $m_s = +1$ and $m_s = -1$ states) [39,40]. Since the intensity of the EPR signal (and, accordingly, the amplitude of the signal of the first derivative) is proportional to the difference in the populations of the levels between which a spin transition occurs with a change in the magnetic quantum number by 1, then the additional excess of the level population $m_s = 0$ over the level population $m_s = +1$ under quasi-stationary illumination leads to an increase in microwave absorption and the integrated intensity of the EPR line under conditions corresponding to resonance. Here this means that the energy of a microwave radiation quantum is equal to the splitting between the corresponding levels in a magnetic field.

Using to illuminate a xenon lamp's radiation, which has passed through a R64 filter, does not change the intensity of the EPR lines of the $NV^{(-)}$- centers compared to the dark conditions (Fig. 6, *a*, curve *2*). Long-wavelength radiation with $\lambda \geq 640$ nm, therefore, does not cause the effect of optical spin polarization, although the cutoff edge of the R64 filter approximately coincides with the position of the zero-phonon line of the $NV^{(-)}$-center at 638 nm (30.5% transmission at $\lambda = 638$ nm). The use of radiation passed through the L42 filter ($\lambda \geq 420$ nm), on the contrary, demonstrates the same effect of amplification of the EPR lines of the $NV^{(-)}$- center, as in the case of using broadband filter HA30 (Fig. 6, *a*, curve *3* and Fig. 6, *b*, curve *3*). It can be concluded that the main effect in the observed effect is exerted by light with photon energies from 2 to 3 eV.

The observed effect of enhancing the intensity of EPR lines was previously noted in the literature for low-field lines of allowed $\Delta m_s = 1$ transitions and was associated with a change in the populations of sublevels of the triplet state in a magnetic field under optical pumping [38], however, in this study, the same effect is observed for the $\Delta m_s = 2$ transitions in a half magnetic field. In addition, in the experiment, the diamond powder was placed at the bottom of a quartz EPR tube with an inner diameter of ~ 4 mm, and it can be assumed that only the outer layers of the powder ($\sim 25-30\%$ of the material) adjacent to the tube walls are involved in the formation of an additional EPR signal associated with optical spin polarization. Since the signal from $\Delta m_s = 2$ transitions in the half field undergoes less smearing/broadening with fluctuations in the spin-Hamiltonian parameters of the $NV^{(-)}$-center and a change in the orientation of the centers than signals from allowed $\Delta m_s = 1$ transitions, then the effect observed in powders can possibly be used to identify the occurrence of optical spin polarization in diamond particles with $NV^{(-)}$ and sizes less than 30−35 nm, when signals from $\Delta m_s = 1$ transitions are not observed for fundamental reasons [26]. The latter assumption, however, still requires further study and verification.

Conclusion

Microcrystals of synthetic Ib HPHT diamond with $NV^{(-)}$-centers, in addition to specific features associated with luminescence and EPR signals, demonstrate the effect of

amplification of low-field EPR signals caused by optical spin polarization. This enhancement of absorption is observed both for x, y $\Delta m_s = 1$ and $\Delta m_s = 2$ microwave transitions. This effect can be used to select synthetic diamond microcrystals with NV$^{(-)}$- centers, which have excellent technical characteristics, such as luminescence brightness, low content of foreign metal impurities, low internal stresses and high crystalline lattice quality.

Acknowledgments

V.Yu.O. thanks the Research Center for Micro- and Nanotechnologies of Hosei University (Tokyo, Japan) for providing access to the equipment and the opportunity to conduct experiments on the topic of this work.

Funding

This article was supported by the Russian Science Foundation (agreement 21-12-00264).

Conflict of interest

The authors declare that they have no conflict of interest within the scope of the study presented in this article.

Information on authors contribution

V.Yu. Osipov: setting the problem and carrying out EPR measurements at low temperatures, adjusting the optical system, processing and analyzing spectra, writing an article, K.V. Bogdanov: carrying out luminescence and Raman studies, A. Rampersaud: synthesis of samples and their technological processing, including irradiation with high-energy electrons, K. Takai: calibration of the EPR spectrometer and analysis of EPR spectroscopy data, Y. Ishiguro: operational control of the low-temperature system, vacuum and ventilation lines, temperature stabilization systems, A.V. Baranov: analysis of optical measurement data and editing of the manuscript.

References

[1] A.M. Zaitsev. *Optical properties of diamond: A data handbook* (Springer, Berlin–Heidelberg–New York, 2001). DOI: 10.1007/978-3-662-04548-0
[2] H.C. Chang, W.W.W. Hsiao, M.C. Su. *Fluorescent nanodiamonds* (John Wiley & Sons, Hoboken–Chichester–Oxford, 2019). DOI: 10.1002/9781119477099
[3] M.W. Doherty, N.B. Manson, P. Delaney, F. Jelezko, J. Wrachtrup, L.C. L. Hollenberg. Phys. Rep., **528** (1), 1 (2013). DOI: 10.1016/j.physrep.2013.02.001
[4] J.H.N. Loubser, J.A. van Wyk. Rep. Prog. Phys., **41**, 1201 (1978). DOI: 10.1088/0034-4885/41/8/002
[5] J. Isoya, H. Kanda, J.R. Norris, J. Tang, M.K. Bowman. Phys. Rev. B, **41**, 3905 (1990). DOI: 10.1103/PhysRevB.41.3905
[6] J. Isoya, H. Kanda, Y. Uchida. Phys. Rev. B, **42**, 9843 (1990). DOI: 10.1103/PhysRevB.42.9843
[7] A.T. Collins, H. Kanda, J. Isoya, C.A.J. Ammerlaan, J.A. Van Wyk. Diam. Relat. Mater., **7**, 333 (1998). DOI: 10.1016/S0925-9635(97)00270-7
[8] K. Iakoubovskii, A. Stesmans A. Phys. Status Solidi (a), **186**, 199 (2001). DOI: 10.1103/PhysRevB.66.195207
[9] K. Iakoubovskii, A. Stesmans. Phys. Rev. B, **66** (19), 195207 (2002). DOI: 10.1103/PhysRevB.66.195207
[10] A.T. Collins. Diam. Relat. Mater., **9** (3–6), 417 (2000). DOI: 10.1016/S0925-9635(99)00314-3
[11] V. Nadolinny, A. Komarovskikh, Y. Palyanov. Crystals, **7** (8), 237 (2017). DOI: 10.3390/cryst7080237
[12] V. Nadolinny, A. Komarovskikh, Y. Palyanov, I. Kupriyanov, Y. Borzdov, M. Rakhmanova, O. Yuryeva, S. Veber. Phys. Status Solidi (a), **213** (10), 2623 (2016). DOI: 10.1002/pssa.201600211
[13] I.A. Dobrinets, V.G. Vins, A.M. Zaitsev. *HPHT-treated diamonds: diamonds forever* (Springer, Berlin, Heidelberg, 2013). DOI: 10.1007/978-3-642-37490-6
[14] A. Beveratos, S. Kühn, R. Brouri, T. Gacoin, J.-P. Poizat, P. Grangier. Eur. Phys. J. D, **18** (2), 191 (2002). DOI: 10.1140/epjd/e20020023
[15] F. Jelezko, J. Wrachtrup, Phys. Status Solidi (a), **203**, 3207 (2006). DOI: 10.1002/pssa.200671403
[16] L. Rondin, J.P. Tetienne, T. Hingant, J.F. Roch, P. Maletinsky, V. Jacques. Rep. Prog. Phys., **77** (5), 056503 (2014). DOI: 10.1088/0034-4885/77/5/056503
[17] T. Rosskopf, A. Dussaux, K. Ohashi, M. Loretz, R. Schirhagl, H. Watanabe, S. Shikata, K.M. Itoh, C.L. Degen. Phys. Rev. Lett., **112**, 147602 (2014). DOI: 10.1103/PhysRevLett.112.147602
[18] M. Fujiwara, Y. Shikano. Nanotechnology, **32**, 482002 (2021). DOI: 10.1088/1361-6528/ac1fb1
[19] D.A. Broadway, B.C. Johnson, M.S.J. Barson, S.E. Lillie, N. Dontschuk, D.J. McCloskey, A. Tsai, T. Teraji, D.A. Simpson, A. Stacey, J.C. Mc Callum, J.E. Bradby, M.W. Doherty, L.C.L. Hollenberg, J.-P. Tetienne. Nano Lett., **19** (7), 4543 (2019). DOI: 10.1021/acs.nanolett.9b01402
[20] M.W. Doherty, V.V. Struzhkin, D.A. Simpson, L.P. McGuinness, Y. Meng, A. Stacey, T.J. Karle, R.J. Hemley, N.B. Manson, L.C.L. Hollenberg, S. Prawer S. Phys. Rev. Lett., **112** (4), 047601 (2014). DOI: 10.1103/PhysRevLett.112.047601
[21] AF4. R. Schirhagl, K. Chang, M. Loretz, C.L. Degen. Annu. Rev. Phys. Chem., **65**, 83 (2014). DOI: 10.1146/annurev-physchem-040513-103659
[22] A. Gali. Nanophotonics, **8** (11), 1907 (2019). DOI: 10.1515/nanoph-2019-0154
[23] S. Haziza, N. Mohan, Y. Loe-Mie, A.M. Lepagnol-Bestel, S. Massou, M.P. Adam, X.L. Le, J. Viard, C. Plancon, R. Daudin, P. Koebel, E. Dorard, C. Rose, F.-J. Hsieh, C.-C. Wu, B. Potier, Y. Herault, C. Sala, A. Corvin, B. Allinquant, H.-C. Chang, F. Treussart, M. Simonneau. Nat. Nanotechnol., **12** (4), 322 (2017). DOI: 10.1038/nnano.2016.260
[24] A. Filipkowski, M. Mrózek, G. Stępniewski, J. Kierdaszuk, A. Drabińska, T. Karpate, M. Głowacki, M. Ficek, W. Gawlik, R. Buczyński, A. Wojciechowski, R. Bogdanowicz, M. Klimczak. Carbon, **196**, 10 (2022). DOI: 10.1016/j.carbon.2022.04.024
[25] A.I. Shames, V.Y. Osipov, H.J. von Bardeleben, J.P. Boudou, F. Treussart, A.Y. Vul'. Appl. Phys. Lett., **104** (6), 063107 (2014). DOI: 10.1063/1.4865205

[26] A.I. Shames, V.Y. Osipov, J.P. Boudou, A.M. Panich, H.J. von Bardeleben, F. Treussart, A.Y. Vul'. J. Phys. D: Appl. Phys., **48** (15), 155302 (2015). DOI: 10.1088/0022-3727/48/15/155302
[27] V.Y. Osipov, K.V. Bogdanov, F. Treussart, A. Rampersaud, A.V. Baranov.Opt. and spectr. **130** (2), 332 (2022). DOI: 10.21883/OS.2022.02.52004.2872-21
[28] L. Dei Cas, S. Zeldin, N. Nunn, M. Torelli, A.I. Shames, A.M. Zaitsev, O. Shenderova. Adv. Funct. Mater., **29** (19), 1808362 (2019). DOI: 10.1002/adfm.201808362
[29] O.A. Shenderova, A.I. Shames, N.A. Nunn, M.D. Torelli, I. Vlasov, A. Zaitsev. J. Vac. Sci. Technol. B: Nanotechnol. Microelectron., **37** (3), 030802 (2019). DOI: 10.1116/1.5089898
[30] A.I. Shames, V.Y. Osipov, K.V. Bogdanov, A.V. Baranov, M.V. Zhukovskaya, A. Dalis, S.S. Vagarali, A.J. Rampersaud. J. Phys. Chem. C, **121** (9), 5232 (2017). DOI: 10.1021/acs.jpcc.6b12827
[31] K.V. Bogdanov, M.V. Zhukovskaya, V.Yu. Osipov, E.V. Ushakova, M.A. Baranov, K. Takai, A. Rampersaud, A.V. Baranov. APL Materials, **6** (8), 086104 (2018). DOI: 10.1063/1.5045535
[32] V.Yu. Osipov, N.M. Romanov, K.V. Bogdanov, F. Treussart, C. Jentgens, A. Rampersaud. J. Opt. Technol., **85** (2), 63 (2018). DOI: 10.1364/JOT.85.000063
[33] S.D. Subedi, V.V. Fedorov, J. Peppers, D.V. Martyshkin, S.B. Mirov, L. Shao, M. Loncar. Opt. Mater. Express, **9** (5), 2076 (2019). DOI: 10.1364/OME.9.002076
[34] V.Yu. Osipov, F. Treussart, S.A. Zargaleh, K. Takai, F.M. Shakhov, B.T. Hogan, A. Baldycheva. Nanoscale Res. Lett., **14** (1), 279 (2019). DOI: 10.1186/s11671-019-3111-y
[35] W.V. Smith, P.P. Sorokin, I.L. Gelles, G.J. Lasher. Phys. Rev., **115**, 1546 (1959). DOI: 10.1103/PhysRev.115.1546
[36] V.Yu. Osipov, F.M. Shakhov, N.M. Romanov, K. Takai. Mendeleev Commun., **32** (5), 645 (2022). DOI: 10.1016/j.mencom.2022.09.026
[37] K. Jeong, A.J. Parker, R.H. Page, A. Pines, C.C. Vassiliou, J.P. King. J. Phys. Chem. C, **121** (38), 21057 (2017). DOI: 10.1021/acs.jpcc.7b07247
[38] J. Harrison, M.J. Sellars, N.B. Manson. J. Lumin., **107** (1−4), 245 (2004). DOI: 10.1016/j.jlumin.2003.12.020
[39] J.D. Breeze, E. Salvadori, J. Sathian, N.M. Alford, C.W. Kay. Nature, **555** (7697), 493 (2018). DOI: 10.1038/nature25970
[40] S. Felton, A.M. Edmonds, M.E. Newton, P.M. Martineau, D. Fisher, D.J. Twitchen, J.M. Baker. Phys. Rev. B, **79** (7), 075203 (2009). DOI: 10.1103/PhysRevB.79.075203